Check for updates

Conjugation through Si–O–Si bonds, silsesquioxane (SQ) half cage copolymers, extended examples *via* $SiO_{0.5}/SiO_{1.5}$ units: multiple emissive states in violation of Kasha's rule†

Zijing Zhang,[a] Jose Jonathan Rubio Arias,[a] Hana Kaehr,[a] Yujia Liu, [ID][b]
Ryoga Murata,[b] Masafumi Unno, [ID][b] Nuttapon Yodsin,[c] Pimjai Pimbaotham,[d]
Siriporn Jungsuttiwong, [ID][d] Matt Rammo,[e] Jung-Moo Heo,[a] Jinsang Kim, [ID][a]
Aleksander Rebane[f] and Richard M. Laine [ID] *[a]

We previously reported that phenyl- and vinyl-silsesquioxanes (SQs), $[RSiO_{1.5}]_{8,10,12}$ (R = Ph or vinyl) functionalized with three or more conjugated moieties show red-shifted absorption- and emission features suggesting 3-D conjugation *via* a cage centered LUMOs. Corner missing $[PhSiO_{1.5}]_7(OSiMe_3)_3$ and edge opened, end capped $[PhSiO_{1.5}]_8(OSiMe_2)_2$ (double decker, DD) analogs also offer red shifted spectra again indicating 3-D conjugation and a cage centered LUMO. Copolymerization of DD $[PhSiO_{1.5}]_8(OSiMevinyl)_2$ with multiple R–Ar–Br gives copolymers with emission red-shifts that change with degree of polymerization (DP), exhibit charge transfer to F_4TNCQ and terpolymer averaged red-shifts suggesting through chain conjugation even with two (O–Si–O) end caps possibly *via* a cage centered LUMO. Surprisingly, ladder (LL) SQ, $(vinylMeSiO_2)[PhSiO_{1.5}]_4(O_2SiMevinyl)$ copolymers offer emission red-shifts even greater for analogous copolymers requiring a different explanation. Here we assess the photophysical behavior of copolymers of a more extreme SQ form: the half cage $[PhSiO_{1.5}]_4(OSiMe_2Vinyl)_4$, Vy_4HC SQs. We again see small red-shifted absorptions coupled with significant red-shifted emissions, even with just a half cage, thus further supporting the existence of pπ–dπ and/or σ*–π* conjugation through Si–O–Si bonds and contrary to most traditional views of Si–O–Si linked polymers. These same copolymers donate an electron to F_4TCNQ generating the radical anion, F_4TCNQ^- as further proof of conjugation. Column chromatographic separation of short from longer chain oligomers reveals a direct correlation between DP and emission λ_{max} red-shifts as another indication of conjugation. Further, one- and two-photon absorption and emission spectroscopy reveals multiple excited fluorescence-emitting states in a violation of Kasha's rule wherein emission occurs only from the lowest excited state. Traditional modeling studies again find HOMO LUMO energy levels residing only on the aromatic co-monomers rather than through Si–O–Si bonds as recently found in related polymers.

[a]Department of Mater. Sci. and Engin., Macromolecular Science and Eng. Center University of Michigan, Ann Arbor, 48109-21236, USA. E-mail: talsdad@umich.edu
[b]Department of Chemistry and Chemical Biology, Graduate School of Science and Technology Gunma University, Kiryu 376-8515, Japan
[c]Department of Chemistry, Faculty of Science, Silpakorn University, Nakorn Pathom 73000, Thailand
[d]Department of Chemistry and Center of Excellence for Innovation in Chemistry, Faculty of Science, Ubon Ratchathani University, Ubon Ratchathani 34190, Thailand
[e]National Institute of Chemical Physics and Biophysics, Tallinn, Estonia
[f]Montana State University, Bozeman, MT 59717, USA
†Electronic supplementary information (ESI) available. See DOI: https://doi.org/10.1039/d4dt00567h

Introduction

Silsesquioxane (SQ) cages, oligomers and polymers are well recognized to offer a wide variety of properties including high temperature stability, biocompatibility, hydrophobicity, transparency, and insulating properties. Their presence in commercial applications is widespread and the subject of multiple reviews and one book.[1–21] They have been compared to organic decorated silica; however, in multiple papers we demonstrated that T_8, T_{10} and T_{12} phenyl and vinyl SQs functionalized with three or more conjugated moieties demonstrate photophysical properties best explained by formation of a cage centered LUMO conjugated with these appended moieties.[22–32]

Modeling finds cage centered LUMOs in the T_8, T_{10} and T_{12} SQs.[33,34] Modified cages and polymers made from them also

exhibit 3-D conjugation. SQs exposed to intense laser light generate a spherical magnetic field inside the functionalized cages supporting formation of a LUMO.[29]

Efforts to identify limiting structures wherein cage LUMOs do not form led to syntheses of corner missing, doubly open, then "double decker" (DD) and finally ladder (LL) SQs with [O–Si(Mevinyl)–O] endcaps, Scheme 1a.[30,31,35]

Bromination/iodination of all phenyl SQs followed by Heck catalytic cross-coupling, Scheme 1b, gives 4-*R*-stilbene SQs that also exhibit significantly red-shifted emissions *versus* model disiloxane compounds with the same substituents.[35] While main absorption onsets for almost all compounds show very small red-shifts, these may be accompanied by red-shifted lower-intensity features thus deviating from what is expected based on well-studied conjugated organic polymers.

More recently we copolymerized MeVinylSi(O–)$_2$ end-capped DD and LL systems with multiple aromatics per Scheme 1b[31,32] to test conjugation limits using *i.e.* divinyl-benzene tethers building on previous studies wherein phenyl T$_{10}$ and T$_{12}$ cage divinylbenzene copolymers exhibited through chain conjugation.[24]

In particular, we assumed that the absence of a cage in LL SQ copolymers would obviate formation of a cage centered LUMO and therefore conjugation. However both DD and LL SQ copolymers show conjugation even with vinyldisiloxane end caps and *for LL systems without a cage*.[32] In addition to photophysical evidence for conjugation, DD and LL polymers donate electrons to F$_4$TCNQ exhibiting integer electron transfer forming F$_4$TCNQ$^{\cdot-}$; also proof of conjugation. Alternating terpolymers also show red shifted emission averages of the two homo copolymers.[26,36]
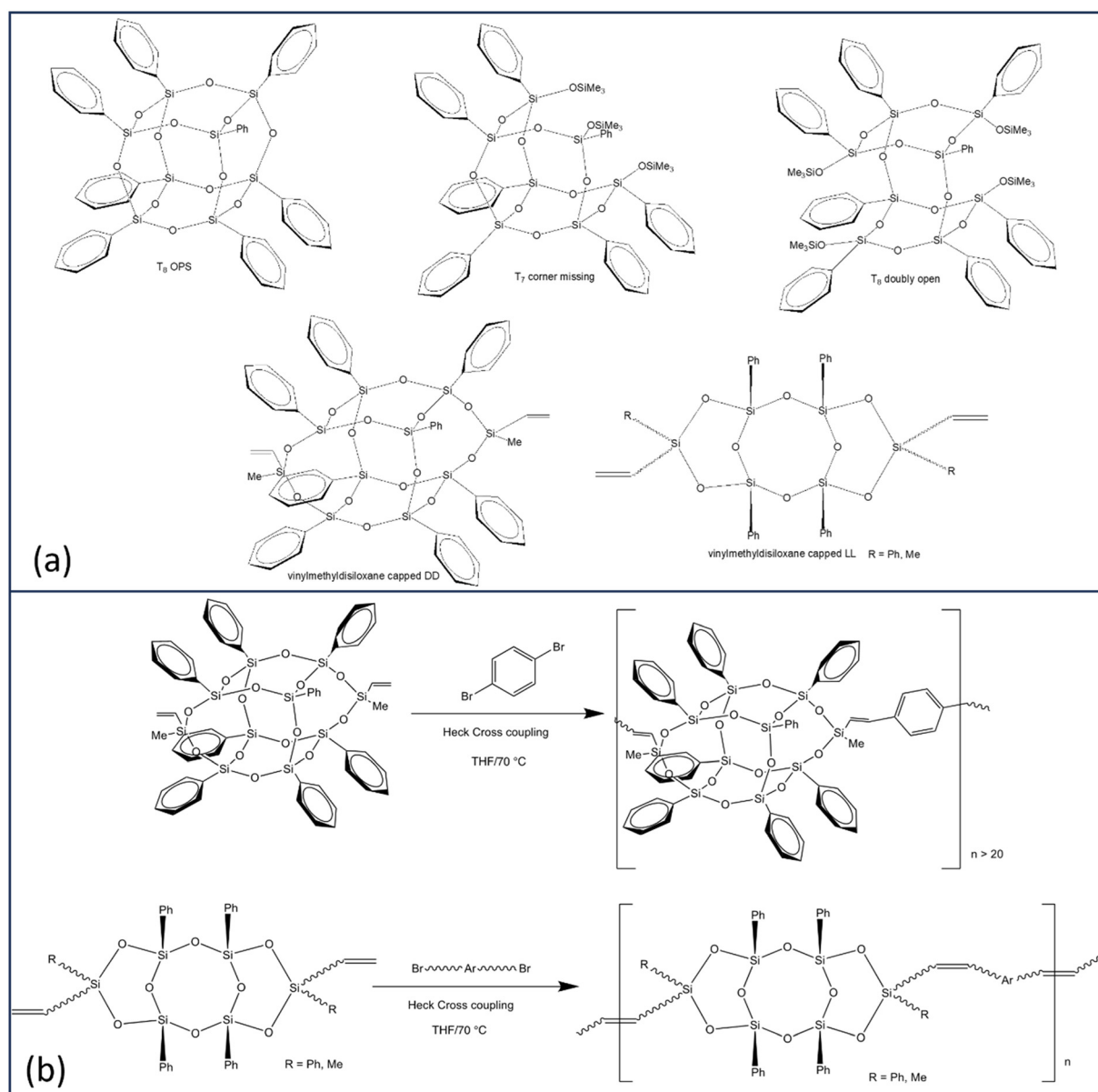
Scheme 1 (a) Selected SQ structural formats. (b) Copolymerization of vinylmethylsiloxane capped DD and LL monomers.
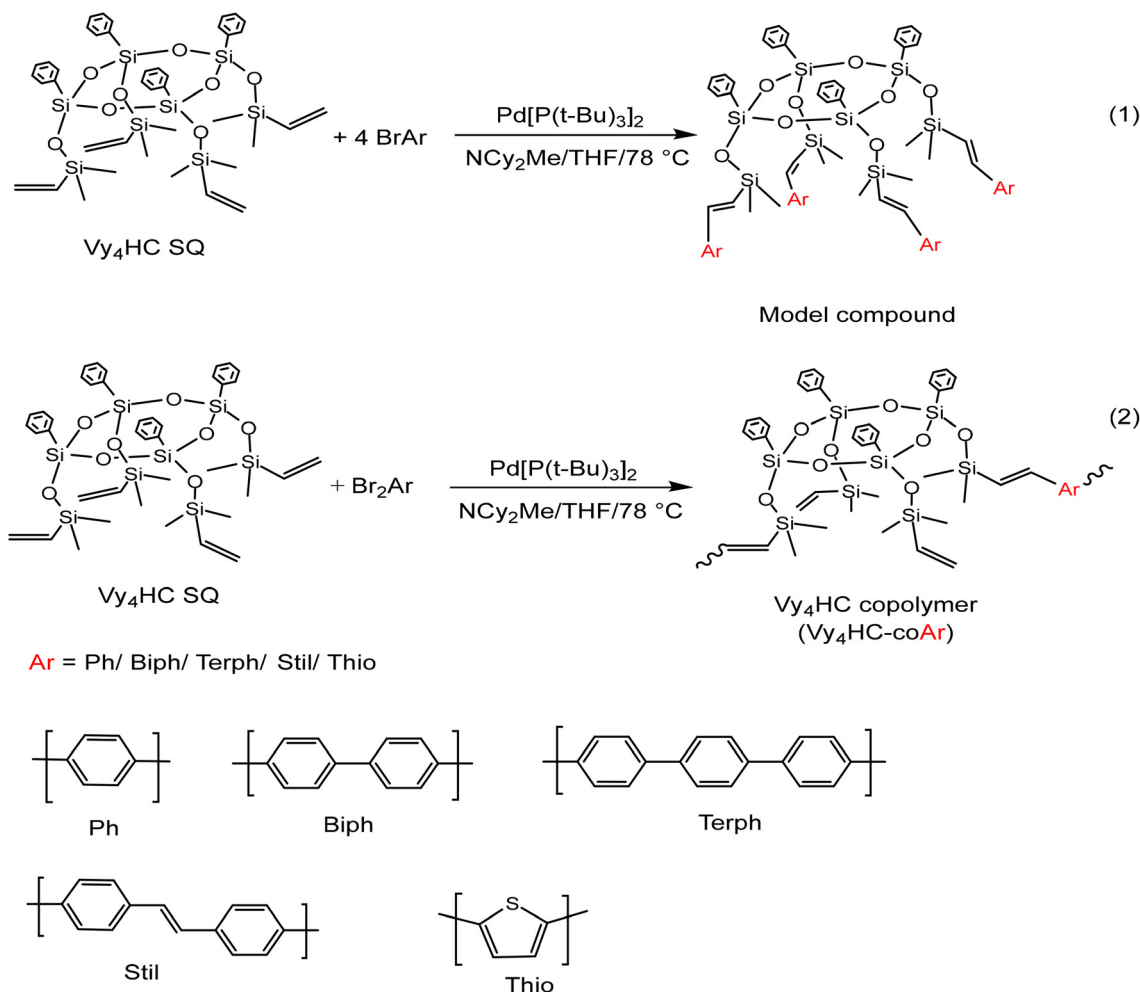
Scheme 2 Vinyldimethylsiloxane capped half cage (Vy$_4$HC) model compound reaction (**1**) and copolymerization reaction (**2**). Ar: selection of aromatic moieties.

Here, we explore further deviations from initial structures searching for limiting siloxane/SQ oligomers/polymers where conjugation is absent. To this end, we synthesized half cages (Vy$_4$HC) capped with pendant OSiMe$_2$Vinyls, Vy$_4$HC, Scheme 2 [37,38] followed by addition of simple monobromo (model compounds) and then dibromo–aromatics (1 : 1 copolymerization) *via* Heck catalytic cross coupling (see experimental) to assess their photophysical properties. We again find conjugation *via* Si–O–Si bonds based on: (1) comparison with model compounds, (2) red-shifted emission λ_{max} *vs.* degree of polymerization (DP), (3) electron transfer to F$_4$TCNQ, and (4) 1PA and 2PA photophysics.

Results and discussion

The objectives of the work reported here are to elaborate on our understanding of "unconventional conjugation" in SQs *via* efforts to identify copolymer systems with backbones consisting in part of Si–O–Si bonds that show photophysical and electrochemical behavior typically associated with conjugation in traditional conjugated organic polymers.[31,39] The approach chosen is to eliminate the cage but retain multiple, pendant Si–O–SiMe$_2$vinyl links, with the idea that making the system look more like a polysiloxane would engender "insulating" properties in copolymers with aromatic and heteroaromatic comonomers.

In the following sections, we first discuss synthesis methods and copolymer characterization, followed by photophysical studies on absorption and emission behavior especially *vs.* DP. Thereafter, complementary studies are undertaken to assess photophysical behavior vis a vis one photon absorption (1PA) and two photon absorption (2PA) spectroscopy in part demonstrating non-Kasha's rule behavior. Then, electron transfer to F$_4$TCNQ studies is used to assess selected copolymers' abilities to donate an electron, essentially a form of doping. Finally, we present an approach to theoretically modeling copolymer behavior and give an estimation of the HOMO LUMO levels using a traditional approach. A conclusions section follows.

Synthesis of Vy$_4$HC-copolymers and model compounds

The first step in these studies was to synthesize model compounds by reacting Vy$_4$HC with four equivalents of Br–Ar (phenyl, biphenyl, stilbene, thiophene). Thereafter, copolymers were synthesized using 1 : 1 molar ratios Vy$_4$HC : Br–Ar–Br typical for condensation polymerization studies. Vy$_4$HC copolymer and model compound syntheses and purification often gives liquids. Chromatography *via* a 5 cm silica gel column allows removal of remaining base and residual catalyst.

Table 1 presents estimated molar masses, and approximate proportions of fractions of eluted products estimated from deconvoluted GPC profiles (Fig. S1–S4†). Fig. S5† displays stacked multimodal GPC traces for Vy$_4$HC copolymers. The GPC traces suggest chain growth is influenced by co-monomer structure with sulfur containing aromatics reacting more slowly because sulfur binds to the catalyst sufficiently strongly to reduce reactivity as seen previously.[26–28] As expected, non-sulfur containing copolymers offer higher average molecular weights (MWs) in accord with our previous reports.[30–32] Copolymer structures are confirmed by Fig. S6–8† MALDI data. As an example, Fig. S9† provides before and after chromatography FTIRs proving base removal. Fig. S10† provides an example ^{1}H NMR of an Vy$_4$HC-copolymer.[30,32,35]

Fig. S11† presents the corresponding Vy$_4$HC copolymer TGAs. Crucial data are summarized in Table 1. The found ceramic yields for the HC copolymers are quite reduced *vs.* those calculated as might be expected given that copolymerization is at 1 : 1 Vy$_4$HC : Br–Ar–Br ratios. Thus, each HC will have two unreacted vinylMe$_2$SiO groups that likely volatilize easily rather than convert to SiO$_2$ on oxidation. The 5% mass degradation temperature ($T_{d\ 5\%}$) for Vy$_4$HC-coStil is notably high enough to consider use for solution processing of electrooptical devices.

Once the copolymers of both systems and their model compounds were reproducibly synthesized and fully characterized, photophysical characterization studies were undertaken at two levels; one consisting of simply evaluating their one photon absorption and emission behavior using traditional Uv-Vis methods followed by more exacting 1PA and 2PA characterization.

Photophysical characterization of Vy$_4$HC-copolymers and model compounds

The copolymers isolated from solution all show emission behavior suggesting both conjugation and differences in band gaps that are comonomer dependent, Fig. S12.† Fig. 1a and b present normalized absorption-emission spectra for Vy$_4$HC-copolymers. Their photophysical parameters are summarized in Table 2. All Vy$_4$HC-copolymers offer significant emission red-shifts in λ_{max} *vs.* model compounds, the Vy$_4$HC-coStil and Vy$_4$HC-coThio are shown as examples in Fig. 1c and d respectively. Individual absorption and emission data for the Vy$_4$HC-copolymer systems are presented in Fig. S13–S17.† Vy$_4$HC-coPh/Biph/Terph show quantum efficiencies (Φ_F) ≥ 70% offering potential for applications in the OLEDs, white light or possibly as hybrid photovoltaic cells.

Note that in Table 2, the model compounds present lower Φ_F, implying oligomerization improves Φ_F perhaps by reducing non-radiative decay processes. Compared to the single aromatics, all Vy$_4$HC-copolymers and model compounds show an increasing molar absorption coefficient, which may arise from the presence of Vy$_4$HC enhancing π to π^* transitions. The excited state lifetimes (in Fig. S18†) of all Vy$_4$HC-copolymers and model compounds are within the scale of ns which indicates quick recombination happens defining luminescence behavior as fluorescence. The radiative constants of all copolymers (in Table S1†), with the exception of coThio, are enhanced, whereas the non-radiative constants are reduced. This suggests that the copolymer systems are likely effective in suppressing non-radiative processes, thereby enhancing photoluminescence (PL) emission.

Example of the effects of DP on photophysics

To further explore conjugation in these compounds, column chromatography was used to separate Vy$_4$HC-coStil fractions, to assess DP effects on photophysical properties. Fig. 2a and b provide optical images of the column separation process and the individual samples collected as elution continues. Table 3 provides detailed absorption, emission and MALDI data. Original MALDI figures of selected eluate samples are shown

---

Table 1 Yields, thermal properties, Mn for co-polymers from GPC and TGA data. GPC results following deconvolution. Estimated Mn's correspond to GPC software calculations using polystyrene standards

Copolymer	Crude yield (%^{M})	GPC						Td$_{5\%}$ (°C)	Theoretical CY (wt%)	Found CY (wt%)
		Greatest MW fraction		2nd MW fraction		3rd MW fraction				
		Mn^a (kg mol^{-1})	(%) total area	Mn^a (kg mol^{-1})	(%) total area	Mn^a (kg mol^{-1})	% total area			
Vy$_4$HC-coThio	94	3.5	72	2.5	5	1.7	15.7	253	50	33
Vy$_4$HC-coPh	82	8.1	1	2.6	68	2.1	16.8	294	50	37
Vy$_4$HC-coBiph	35	15.8	40	6.1	5	3.5	39.9	174	46	34
Vy$_4$HC-coTerph	56	9.9	21	5	22	3.5	49.9	335	43	35
Vy$_4$HC-coStil	77	9.6	4	3.9	82	2.6	0.41	487	45	40

^{a} Estimated from deconvoluted GPC traces, Fig. S1–S4.† CY = ceramic yield, Fig. S11.†
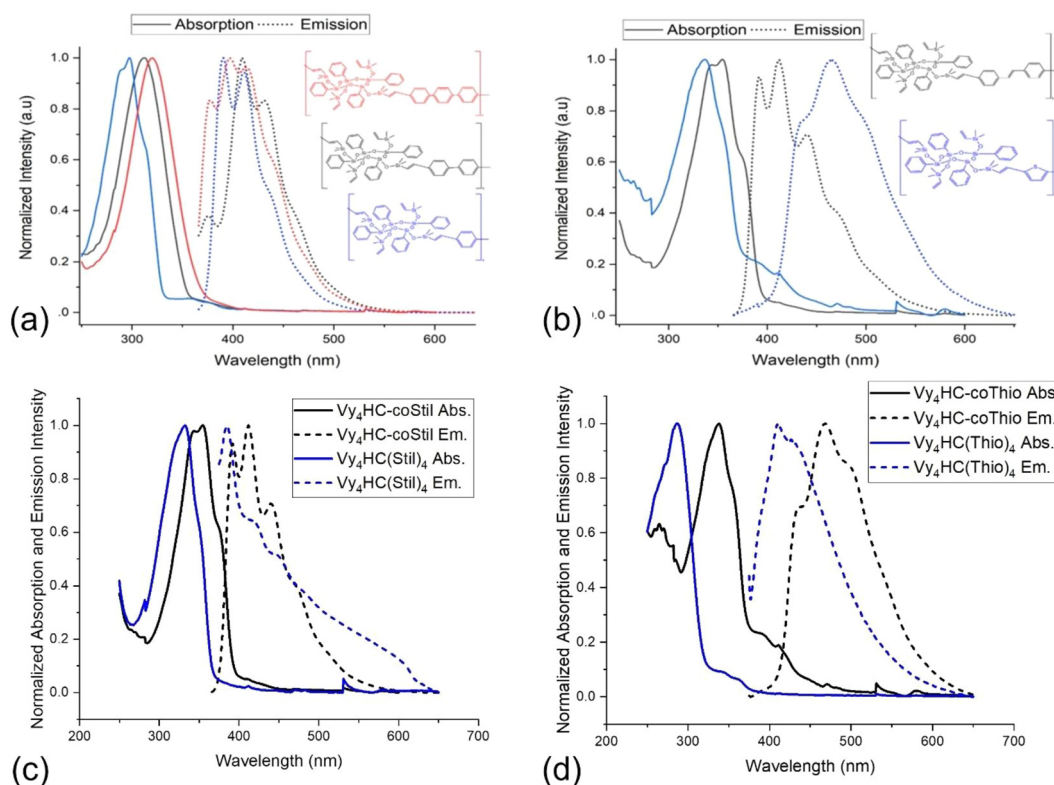
Fig. 1 Normalized absorption (solid line) and emission (dashed line) spectra of (a) Vy$_4$HCco- Ph, Biph and Terph and (b) Vy$_4$HCco-Thio and Stil oligomers in DCM. Excitation wavelength, λ_{ex} = 356 nm. Normalized absorption (solid line) and emission (dashed line) spectra of the model compounds (c) Vy$_4$HC(Stil)$_4$ and (d) Vy$_4$HC(Thio)$_4$ presented along with the corresponding co-polymers Vy$_4$HC-coStil and Vy$_4$HC-coThio in DCM. Excitation wavelength is, λ_{ex} = 356 nm.

Table 2 Photophysical properties of Vy$_4$HC-copolymers and model compounds[a]

		Absorption, λ_{max} (nm)	Emission, λ_{max} (nm)	E_{stokes} (eV)	Molar Absorptivity, ε (L mol^{-1} cm^{-1})	Quantum efficiency, Φ_F (%)	τ_{avg} (ns)
Copolymers	Vy$_4$HC-coPh	289, <u>297</u>	390 411	1.00	23 100	86 ± 1	1.2
	Vy$_4$HC-coBiph	313	<u>409</u>, 432	0.93	33 100	88 ± 1	1.3
	Vy$_4$HC-coTerph	320	415	0.89	48 300	75 ± 1	1.5
	Vy$_4$HC-coStil	344, <u>354</u>	392, <u>412</u>, 440	0.49	58 200	50 ± 3	1.8
	Vy$_4$HC-coThio	338	469	1.03	5900	3.0 ± 0.2	1.2
Model compounds	Vy$_4$HC(Ph)$_4$	252	390, <u>409</u>, 431	1.89	—	0.08 ± 0.01	—
	Vy$_4$HC(Biph)$_4$	288	<u>385</u>, 404	1.09	37 400	3.0 ± 0.5	2.1
	Vy$_4$HC(Stil)$_4$	332	385	0.51	61 200	1.2 ± 0.2	0.1
	Vy$_4$HC(Thio)$_4$	287	412	1.31	—	0.04 ± 0.02	—

[a] Underlined value is λ_{max}; τ_{avg}: average excited state lifetime.

in Fig. S19–S24.† Higher DP materials may also be present but may not ionize efficiently.

Samples marked with a larger number contain oligomers with greater DPs. Color changes under 365 nm irradiation vary from purple to blue to green within the column and isolated samples with increasing DP. In isolated samples, absorption λ_{max} exhibit red-shifts from 277 (monomer) to 354 nm (oligomers) in Fig. 2c. Likewise, emission λ_{max} red-shifts from 307 to 444 nm in Fig. 2d. Table 3 summarizes photophysical behavior of selected samples.

From original half cages to oligomers to hexamers, the absorption λ_{max} red shifts from 277 to 354 nm and the emission λ_{max} shifts from 307 to 470 nm. As the structure changes from Vy$_4$HC to Vy$_4$HC-Stil to Vy$_4$HC-Stil-Vy$_4$HC, λ_{max} absorption red shifts from 277 to 349 to 354 nm. These compounds can be viewed as models. At greater DPs the absorption λ_{max} centers at 344–354 nm.

Comparing HC emission spectra with associated MALDI, the new emission peaks appearing at 409, 444, 470 nm likely result from domination by dimers, then trimers and thereafter
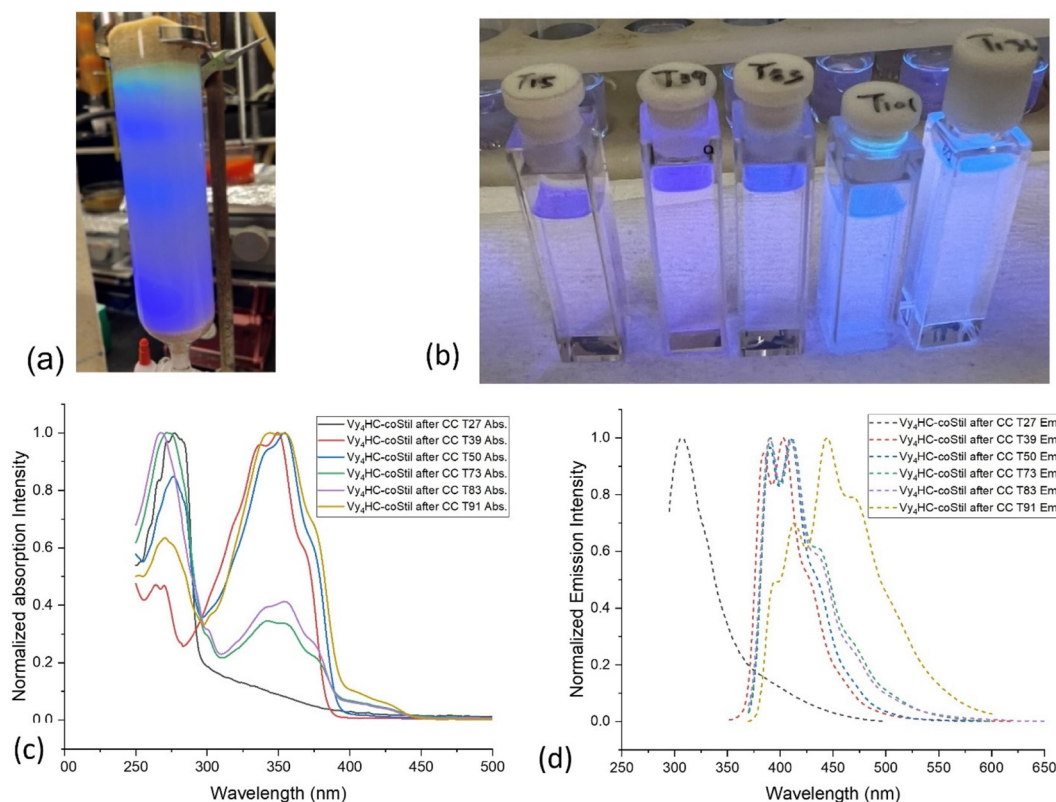
Fig. 2 (a) Optical images of Vy$_4$HC–coStil column illuminated with 365 nm light. Emission changes *vs.* vertical position on column. (b) Fluorescence emitted by selected fractions. Normalized (c) absorption (solid lines) and (d) emission (dashed lines) spectra of selected samples of the Vy$_4$HCcoStil in DCM after column chromatographic separation.

Table 3 Normalized absorption and emission λ_{max} for Vy$_4$HC–coStil oligomers *vs.* DP (DCM)

Sample	Abs. (nm)	Em. (nm)	MALDI[a]
27	277	307	Vy$_4$HC
39	263, 270, 337, <u>349</u>	385, <u>402</u>	Vy$_4$HC-Stil
50	276, 343, <u>354</u>	391, <u>409</u>	Dimers
73	<u>273</u>, 342, 355	<u>391</u>, <u>409</u>, 435 (shoulder)	<u>Dimers</u>, trimers
83	<u>267</u>, 342, 355	<u>391</u>, <u>409</u>, 435(shoulder)	Dimers, <u>trimers</u>
91	270, <u>344</u>, <u>354</u>	394, 413, <u>444</u>, 470	Dimers, <u>trimers</u>, <u>tetramers</u>, pentamers, hexamers

[a] Fig. S19–S24,† underlined peaks are λ_{max}.

tetramers. These results offer additional proof of DP dependent extended conjugation, a typical result for conjugated polymers. A series of relatively weak absorption peaks located at 260–280 nm likely derive from vibronic progression of the attached phenyl groups.

Complementary to the more traditional UV-vis absorption and emission studies above, it was also important to explore photophysics in more detail given the unexpected behavior of these new copolymers, hence the following efforts.

2D excitation–emission spectral maps

Kasha's rule states that on photoexcitation, molecules/polymers in the excited state can be expected to relax to the lowest energy excited state before relaxing to the ground state with

coincident emission of a lower energy photon.[40,41] A majority of the polymers synthesized here seem to violate this rule as exemplified by the following.

Vy$_4$HC-coStil was chosen as an example to explore its photophysics in further detail by measuring 2D excitation–emission spectral maps for both one-photon excited fluorescence (1PEF) and two-photon excited fluorescence (2PEF).

Fig. 3a and b present the one-photon 2D spectral map for Vy$_4$HC-coStil in ACN spanning the excitation wavelengths, λ_{ex} = 200–550 nm (vertical axis), and the emission wavelengths, λ_{em} = 230–700 nm (horizontal axis). The diagonal lines are spectrometer artifacts corresponding to the 1st and 2nd diffraction order Rayleigh scattering. Weaker lines are Raman scattering from the solvent. When both the excitation and emission wave-
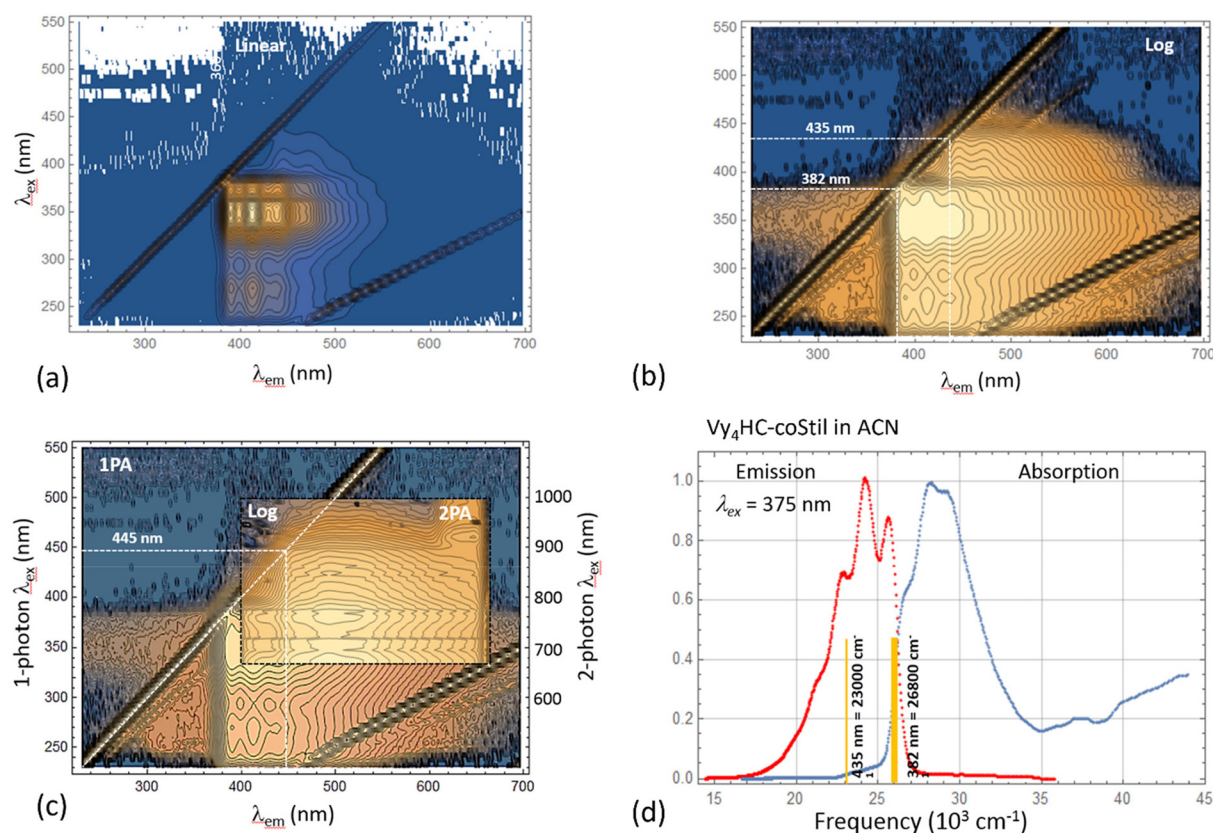
Fig. 3 Emission spectrum of Vy₄HC-coStil in acetonitrile in the range, λ_{em} = 230–700 nm (horizontal axis) plotted as function of excitation wavelength, λ_{ex} = 230–550 nm (vertical axis); the emission intensity shown on (a) linear scale and (b) logarithmic scale. Diagonal lines are spectrometer artifacts at, $\lambda_{em} = \lambda_{ex}$, and $\lambda_{em} = 2\lambda_{ex}$. (c) Log-scale 2D emission spectrum of Vy₄HC-coStil in DMSO obtained by 1-photon (main panel) and by 2-photon excitation (insert). Right vertical axis shows 2-photon excitation range, λ_{ex} = (2PA) = 680–1000 nm. Vertical and horizontal dashed lines indicate the location of origin at 445 nm. Diagonal dashed line shows $\lambda_{em} = \lambda_{ex}$. (d) Summary of characteristic features of absorption- and emission spectra of Vy₄HC-coStil in ACN. Blue curves – normalized absorption spectrum; Red curve –normalized emission spectrum at λ_{ex} = 375 nm. Vertical bars show the frequency of different origins observed in the 1-photon 2D excitation emission.

lengths approach, $\lambda_{em} \sim \lambda_{ex}$, ~382 nm, a distinct features called "origin" can be observed corresponding to the excited energy level that emits fluorescence with only a minimal amount of Stokes shift. Normally, *i.e.* when Kasha's rule is fulfilled, each type of fluorophore shows only one such origin. However, when the same data is presented as a logarithmic intensity scale, Fig. 3b, then a second weaker origin at 435 nm is also observed. This feature appears to correspond in the linear absorption spectrum of Vy₄HC-coStil (Fig. 1d) to a relative weak but distinct red-shifted shoulder at λ_{1PA} = 400–450 nm. Multiple origins were observed in several systems studied here which indicates the presence of systematic non-Kasha behavior in Vy₄HC-copolymers. It should also be noted that similar excitation- and emission features have been observed previously, even though in variable degrees, in other related polymers, as well as in some model compounds.[31]

Complementing (linear) one-photon spectroscopy with nonlinear two-photon absorption spectroscopy is often advantageous because juxtaposition of the two alternative pathways between the ground- and excited state allows better revealing potential underlying symmetries.[42] Fig. 3c (insert) shows the

2-photon excited 2D emission intensity map of Vy₄HC-coStil dissolved in DMSO. The 2-photon excitation wavelengths cover the range, λ_{2PA} = 680–1000 nm, and are shown on the right vertical axis using the corresponding 1-photon transition wavelength scale, λ_{ex} = 340–500 nm. The corresponding emission wavelength is shown on the horizontal axis, λ_{em} = 400–660 nm. To better compare the 2PEF and 1PEF spectra, the 2-photon measurement is superimposed over the underlying 1PEF 2D spectra map of Vy₄HC-coStil in DMSO but spanning a broader range of wavelengths. The 2-photon excitation map reveals qualitatively similar features as the corresponding 1-photon case; however, the lower-energy origin at ≈445 nm displays a relatively even higher intensity which we may attribute to ~10 nm red-shifted 1PA version of the 435 nm origin. It could serve to indicate a lower-energy electronic transition accompanied by an increasingly larger change of the permanent electric dipole moment.[43] Even though the exact nature of associated excited electronic states is currently under discussion, it is remarkable that the 2- photon excitation produces a picture that is, in many respects, similar to that observed in the 1-photon excitation. In particular, the appear-

ance of an origin in the 2-photon spectral map indicates that the excited species most likely lack center(s) of inversion because otherwise the emission would emanate from a different excited state.

Fig. 3d summarizes the most prominent features of origins observed in the absorption- and emission spectra of Vy$_4$HC-coStil (right) in ACN. To facilitate better comparison of the corresponding transition energies, the spectra are plotted using the cm^{-1} frequency scale. In this case, the data shows a higher-energy origin at 26 800 cm^{-1}, which could be associated with chromophore-centered vibronic transitions. In addition, there exist origins at 23 000 cm^{-1} pointing at lower-energy excited state (or states). The fact that these low-lying and often only weakly absorbing features appear to be responsible for highly efficient emission *e.g.* Φ_F = 88% in Vy$_4$HC-coBiph, indicate that role of any potential highly fluorescent aggregates or impurities in this unusual behavior is most likely insignificant.

Charge transfer (CT)

Given the unusual nature of the compounds developed in these studies, further proofs are needed to give credence to the proposed existence of conjugation *via* Si–O–Si bonds as a stepping-stone towards the modeling studies below. Hence our efforts to demonstrate CT behavior.

Optoelectronic devices require CT between an electron donor and an acceptor. CT would be in response to absorption of a photon and subsequent electron excitation (photovoltaics) or to an applied potential and subsequent photon emission (OLEDs). To find practical applications for developed materials as reported here, demonstrating CT is of utmost importance. CT can be proven by mixing materials with a strong electron donor, *e.g.* F$_4$TCNQ. DCM solutions of the co-polymer and F$_4$TCNQ mixed at ambient (0.5 h) lead to visible CT changes (Fig. S25†).

Table 4 Charge transfer studies between Vy$_4$HC co-polymers with F$_4$TCNQ

	F$_4$TCNQ Mol %	Cyano- ν(C≡N)	CT degree (δ)
Vy$_4$HC-coPh	50	2192	~1
Vy$_4$HC-coBiph	50	2196	~1
Vy$_4$HC-coTerph	50	2221, 2195	0.18, ~1
Vy$_4$HC-coStil	50	2222, 2210, 2196	015, 0.52, ~1
Vy$_4$HC-coThio	50	2222, 2189	0.15, ~1
F$_4$TCNQ		2227	0

As demonstrated previously, CT can be observed *via* FTIR, UV-vis absorption spectra and to some extent, it is reflected in a change of color to green even brown (color of anionic F$_4$TCNQ).[32] FTIR spectra for Vy$_4$HC copolymers doped with F$_4$TCNQ are shown in Fig. S26.†

On doping with 50$_{mol}$% F$_4$TCNQ, for Vy$_4$HC-coPh and Vy$_4$HC-coBiph, νC≡N band shifts from 2227 to 2194 cm^{-1} are observed for the strongest νC≡N bands of anionic F$_4$TCNQ, indicating integer charge transfer, error in peak value is likely attributable to peak width. Integer charge transfer allows estimating copolymer HOMOs if it is higher than the LUMO of F$_4$TCNQ at −5.3 eV. Vy$_4$HCcoTerph, Vy$_4$HC-coStil and Vy$_4$HC-coThio show both partial and integer CT, the degree of partial CT is presented in Table 4 below. Eqn (1) permits calculation of CT degree.

$$\delta = \frac{2\Delta\nu}{\nu_0}\left[1 - \frac{\nu_1^2}{\nu_0^2}\right]^{-1} \tag{1}$$

ν_1: νC≡N band value of anionic F$_4$TCNQ, 2194 cm^{-1}.
ν_0: νC≡N band value of neutral F$_4$TCNQ, 2227 cm^{-1}.
$\Delta\nu$: νC≡N band shift value.

Absorption spectra for F$_4$TCNQ + Vy$_4$HC-copolymers are shown in Fig. S27.† The absorption peaks at 760 and 860 nm for anionic F$_4$TCNQ correspond to the D$_0$ → D$_1$ transition and are seen for all copolymers with different intensities which indicates varying doping efficiencies.

Modeling studies

As we discovered previously, traditional modeling approaches cannot explain the photophysical results we find with these molecules. Thus, the optimized structures in Fig. S28† represent a starting point for modeling studies using Gaussian 16 methods.

As with our previous publications,[32,35] examples of calculated HOMO and LUMO for Vy$_4$HC-copolymers systems and corresponding absorption spectra presented in Fig. S29–33† indicate localization on aromatic components belying the above evidence of extended conjugation. This extends to calculated emission behavior. Furthermore, we observe that the trends exhibited by the adsorption spectra align with those observed in experimental studies, as tabulated in Table 5. We are still working to establish more encompassing modeling approaches that are ongoing.

In a recently published paper, using a different modeling approach, we were able to determine the existence of dπ–pπ and/or σ*–π* enables conjugation *via* Si–O–Si bonds.[44]

Table 5 Summary calculated photophysical characteristics of Vy$_4$HC co-polymers

Molecules	Abs.$_{exp}$, λ_{max} (nm)	Abs.$_{calc}$, λ_{max} (nm)	Transition	HOMO, LUMO, E_{gap}
Vy$_4$HC-coStil	354	323.09	HOMO→LUMO (96%)	−6.64, −0.58, 6.05
Vy$_4$HC-coThio	335	273.32	HOMO→LUMO (96%)	−7.20, −0.11, 7.09
Vy$_4$HC-coTerph	320	289.22	HOMO→LUMO (91%)	−6.90, −0.29, 6.61
Vy$_4$HC-coBiph	312	275.06	HOMO→LUMO (95%)	−7.07, −0.16, 6.91
Vy$_4$HC-coPh	297	247.86	HOMO→LUMO (88%)	−7.43, 0.13, 7.56
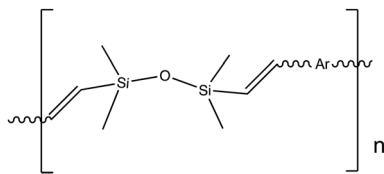
Ar = Ph, Biphenyl, terphenyl, thiophene, etc

Scheme 3 Polysiloxane copolymers also show conjugation likely $d\pi-p\pi$ and/or $\sigma^*-\pi^*$.[45]

Conclusions

Above, we continue to attempt to define the extent of and source of unexpected conjugation in siloxane and SQ compounds linked by vinylMe$_2$Si–O–SiMe$_2$vinyl tethers exploring unique configurations attempting to identify limiting structures; again, finding conjugation. In the examples presented here, we identify conjugation both by red-shifts in emission in 1PA and 2PA studies, charge transfer from polymeric species to the electron acceptor F$_4$TCNQ, correlation of degrees of polymerization (DPs) with extent of red-shift. We also find unexpected failures of Kasha's rule in that many of the compounds studied exhibit multiple emitting states, an uncommon feature of conjugated polymers. These studies have provided the basis for next generation studies on simple polysiloxane copolymers of the type shown in Scheme 3.

Author contributions

R.M. Laine conceived of experiments, directed synthetic efforts and co-wrote the manuscript. Z.Z., J.J.R.A. and H.K. conducted experiments at UM. M.U. and Y.L. conceived of experiments, directed synthesis efforts and co-wrote the manuscript and R.M. conducted syntheses done at Gunma University. S.J. conceived of experiments, directed modeling efforts and N.Y. and P.P. conducted the modeling experiments at Ubon Ratachani and Silpakorn Universities; A.R. conceived of and directed experiments and co-wrote the manuscript, M.R. conducted experiments at Montana State and at National Institute of Chemical Physics and Biophysics. J.H. and J.K. conducted the excited state lifetime measurement at UM.

Conflicts of interest

There are no conflicts to declare.

Acknowledgements

References

1 M. G. Voronkov and V. I. Lavrent'yev, in *Inorganic Ring Systems*, Springer Berlin Heidelberg, Berlin, Heidelberg, 1982, vol. 102, pp. 199–236.

2 J. J. Schwab, J. D. Lichtenhan, K. P. Chaffee, P. T. Mather and A. Romo-Uribe, *MRS Proc.*, 1998, **519**, 21.

3 R. H. Baney, M. Itoh, A. Sakakibara and T. Suzuki, *Chem. Rev.*, 1995, **95**, 1409–1430.

4 G. Calzaferri, in *Tailor-made Silicon-Oxygen Compounds*, Friedr. Vieweg & SohnmbH, 1996, pp. 149–169.

5 J. Lichtenhan, in *Polymeric Materials Encyc*, CRC Press, NY, 1996, vol. 10, pp. 7768–7777.

6 A. Provatas and J. G. Matisons, in *Trends Polym. Sci*, 1997, vol. 5, pp. 327–322.

7 G. Li, L. Wang, H. Ni and C. U. Pittman Jr., *J. Inorg. Organomet. Polym.*, 2001, **11**, 123–154.

8 R. Duchateau, *Chem. Rev.*, 2002, **102**, 3525–3542.

9 Y. Abe and T. Gunji, *Prog. Polym. Sci.*, 2004, **29**, 149–182.

10 S. H. Phillips, T. S. Haddad and S. J. Tomczak, *Curr. Opin. Solid State Mater. Sci.*, 2004, **8**, 21–29.

11 R. Y. Kannan, H. J. Salacinski, P. E. Butler and A. M. Seifalian, *Acc. Chem. Res.*, 2005, **38**, 879–884.

12 R. M. Laine, *J. Mater. Chem.*, 2005, **15**, 3725.

13 P. D. Lickiss and F. Rataboul, in *Advances in Organometallic Chemistry*, Elsevier, 2008, vol. 57, pp. 1–116.

14 K. L. Chan, P. Sonar and A. Sellinger, *J. Mater. Chem.*, 2009, **19**, 9103.

15 J. Wu and P. T. Mather, *Polym. Rev.*, 2009, **49**, 25–63.

16 D. B. Cordes, P. D. Lickiss and F. Rataboul, *Chem. Rev.*, 2010, **110**, 2081–2173.

17 R. M. Laine and M. F. Roll, *Macromolecules*, 2011, **44**, 1073–1109.

18 *Applications of polyhedral oligomeric silsesquioxanes*, ed. C. Hartmann-Thompson, Springer, Dordrecht, 2011.

19 J. Guan, Z. Zhang and R. M. Laine, *Macromolecules*, 2022, **55**, 5403–5411.

20 Y. Du and H. Liu, *ChemCatChem*, 2021, **13**, 5178–5190.

21 M. Soldatov and H. Liu, *Prog. Polym. Sci.*, 2021, **119**, 101419.

22 S. Sulaiman, J. Zhang, T. Goodson III and R. M. Laine, *J. Mater. Chem.*, 2011, **21**, 11177.

23 S. Sulaiman, A. Bhaskar, J. Zhang, R. Guda, T. Goodson and R. M. Laine, *Chem. Mater.*, 2008, **20**, 5563–5573.

24 M. Z. Asuncion and R. M. Laine, *J. Am. Chem. Soc.*, 2010, **132**, 3723–3736.

25 J. H. Jung and R. M. Laine, *Macromolecules*, 2011, **44**, 7263–7272.

26 J. H. Jung, J. C. Furgal, S. Clark, M. Schwartz, K. Chou and R. M. Laine, *Macromolecules*, 2013, **46**, 7580–7590.

27 J. C. Furgal, J. H. Jung, S. Clark, T. Goodson and R. M. Laine, *Macromolecules*, 2013, **46**, 7591–7604.

28 J. C. Furgal, J. H. Jung, T. Goodson and R. M. Laine, *J. Am. Chem. Soc.*, 2013, **135**, 12259–12269.

29 J. Guan, K. Tomobe, I. Madu, T. Goodson, K. Makhal, M. T. Trinh, S. C. Rand, N. Yodsin, S. Jungsuttiwong and R. M. Laine, *Macromolecules*, 2019, **52**, 4008–4019.

30 J. Guan, K. Tomobe, I. Madu, T. Goodson, K. Makhal, M. T. Trinh, S. C. Rand, N. Yodsin, S. Jungsuttiwong and R. M. Laine, *Macromolecules*, 2019, **52**, 7413–7422.

31 J. Guan, J. J. R. Arias, K. Tomobe, R. Ansari, M. de F. V. Marques, A. Rebane, S. Mahbub, J. C. Furgal, N. Yodsin, S. Jungsuttiwong, D. Hashemi, J. Kieffer and R. M. Laine, *ACS Appl. Polym. Mater.*, 2020, **2**(9), 3894–3907.

32 J. Guan, Z. Sun, R. Ansari, Y. Liu, A. Endo, M. Unno, A. Ouali, S. Mahbub, J. C. Furgal, N. Yodsin, S. Jungsuttiwong, D. Hashemi, J. Kieffer and R. M. Laine, *Angew. Chem., Int. Ed.*, 2021, **60**, 11115–11119.

33 R. M. Laine, S. Sulaiman, C. Brick, M. Roll, R. Tamaki, M. Z. Asuncion, M. Neurock, J.-S. Filhol, C.-Y. Lee, J. Zhang, T. Goodson, M. Ronchi, M. Pizzotti, S. C. Rand and Y. Li, *J. Am. Chem. Soc.*, 2010, **132**, 3708–3722.

34 M. Bahrami, H. Hashemi, X. Ma, J. Kieffer and R. M. Laine, *Phys. Chem. Chem. Phys.*, 2014, **16**, 25760–25764.

35 J. Guan, K. Tomobe, I. Madu, T. Goodson, K. Makhal, M. T. Trinh, S. C. Rand, N. Yodsin, S. Jungsuttiwong and R. M. Laine, *Macromolecules*, 2019, **52**, 4008–4019.

36 Z. Zhang, J. Guan, R. Ansari, J. Kieffer, N. Yodsin, S. Jungsuttiwong and R. M. Laine, *Macromolecules*, 2022, **55**(18), 8106–8116.

37 Y. Liu, N. Takeda, A. Ouali and M. Unno, *Inorg. Chem.*, 2019, **58**, 4093–4098.

38 H. Endo, N. Takeda and M. Unno, *Organometallics*, 2014, **33**, 4148–4151.

39 R. M. Laine, *Chem. Commun.*, 2022, **58**, 10596–10618.

40 J. C. Del Valle and J. Catalán, *Phys. Chem. Chem. Phys.*, 2019, **21**, 10061–10069.

41 A. P. Demchenko, V. I. Tomin and P.-T. Chou, *Chem. Rev.*, 2017, **117**, 13353–13381.

42 C. W. Stark, M. Rammo, A. Trummal, M. Uudsemaa, J. Pahapill, M. Sildoja, S. Tshepelevitsh, I. Leito, D. C. Young, B. Szymański, O. Vakuliuk, D. T. Gryko and A. Rebane, *Angew. Chem., Int. Ed.*, 2022, **61**, e202212581.

43 A. Rebane, N. S. Makarov, M. Drobizhev, B. Spangler, E. S. Tarter, B. D. Reeves, C. W. Spangler, F. Meng and Z. Suo, *J. Phys. Chem. C*, 2008, **112**, 7997–8004.

44 J. J. R. Arias, Z. Zhang, M. Takahashi, P. Mahalingam, P. Pimbaotham, N. Yodsin, M. Unno, Y. Liu, S. Jungsuttiwong, J. Azoulay, M. Rammo, A. Rebane and R. M. Laine, *Polym. J.*, 2024, **56**, 577–588.

45 Z. Zhang, H. Kaehr and R. M. Laine, 2023, unpublished work.